Analysis of the Coaxial Helical-Groove Slow-Wave Structure

Guofen Yu, Wenxiang Wang, Yanyu Wei, and Shenggang Liu

***Abstract*—The coaxial helical-groove structure is presented and analyzed in this paper. The dispersion equation and coupling impedance of the structure are given. Numerical calculations of the dispersion relation and coupling impedance with different structure dimensions are carried out. Calculated results indicate that the cold bandwidth of this structure can reach 60%, while the coupling impedance is more than 16 Ω. It shows that the coaxial helical groove is a wide-band slow-wave structure with high-power capacity.**

***Index Terms*—Coaxial helical-groove slow-wave structure, coupling impedance, dispersion relation, slow-wave structure.**

I. Introduction

As a key component of beam-wave interaction in a traveling-wave tube (TWT), the slow-wave circuit directly influences the TWT's characteristics. It influences not only the TWT's operation bandwidth, but also its power capacity. In most cases, there is conflict between the bandwidth and power capacity. This problem is to some extent linked to the openness of the slow-wave system [1]. A wider bandwidth requires an increase in the openness within a certain dimensional range. On the other hand, to improve heat dissipation and to increase the power capacity requires more closeness with the metal envelope. Therefore, the often used slow-wave system, helix or coupled cavity, is of either broad bandwidth or high-power capacity. With the development of recent technological innovations, some larger power helix TWTs [2]–[6] and middle-band coupled-cavity TWTs [7] have been built. However, these devices do not completely meet the need of development of high-power and broad-band TWTs. Thus, seeking a new slow-wave structure possessing broader bandwidth and higher power capacity simultaneously is still very important.

The new structure presented in this paper is a coaxial helical-groove one, as shown in Fig. 1. It is an all-metal circuit. Therefore, it possesses properties such as large size, good heat dissipation, and so on. As it is a coaxial system, its lower cutoff frequency is zero. Therefore, it can be a broad-band and high-power circuit.

The ordinary helical-groove waveguide was studied both in slow- and fast-wave regimes [8]–[11]. The helical-groove system with an inner conductor was also analyzed [12]. However, to the best of the authors' knowledge, no reports about the coaxial helical-groove system have been seen up to now. In this paper, this structure was analyzed in the slow-wave regimes. The expressions of dispersion relation and coupling impedance of the coaxial helical-groove structure have been obtained by using the field-matching method. These expressions are general ones, and they can be easily changed into those of its special cases, i.e., a helical groove [10], helical groove with an inner conductor [12], and helical groove with an outer cylinder (no report was seen by the authors of this paper). Intensive calculations of the obtained dispersion relation and coupling impedance with a variety of structure dimensions have been carried out. This paper is organized as follows. Section I presents a brief introduction. Section II presents the field expressions in the circuit and the relations between the cylindrical and helical coordinate systems. Sections III and IV deal with the derivation of the dispersion equation and the coupling impedance, respectively. Numerical results and discussions are presented in Section V. A short conclusion is presented in Section VI. Finally, dispersion relations, expressions of longitudinal electric fields, and power flows for the three special structures mentioned above are presented in the Appendix.

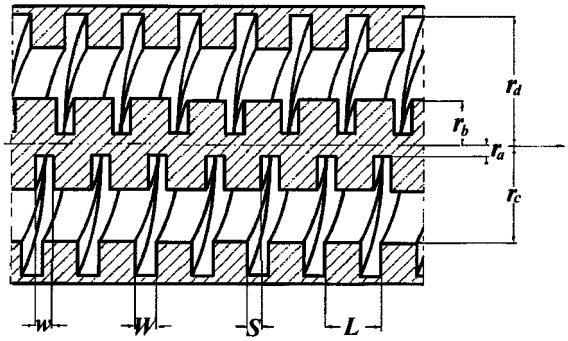

Fig. 1. Configuration of a coaxial helical-grove circuit.

II. Fields in the Coaxial Helical-Groove Circuit

As shown in Fig. 1, r_a, r_b, and w are the inner and outer radii and groove width of the inner groove, respectively. While r_c, r_d, and W are the inner and outer radii and groove width of the outer groove, respectively. S refers to the relative displacement in the longitudinal direction between the inner and outer grooves. We assume that the inner and outer grooves have the same period L. Expressed in terms of cylindrical coordinates r, ϕ, z, the space of the coaxial helical-groove structure can be divided into the following three regions.

Manuscript received May 25, 1999; revised November 8, 2000.

The authors are with the Institute of High Energy Electronics, University of Electronic Science and Technology of China, Chengdu, Sichuan 610054, China.

Publisher Item Identifier S 0018-9480(02)00740-8.

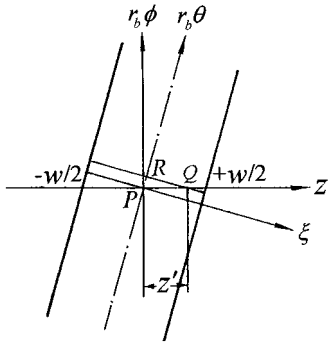

Fig. 2. Diagram for the relation between cylindrical and helical coordinate systems on surface $r = r_b$.

- Region I, the inner groove space

$$\begin{aligned} r_a \le & r \le r_b \\ \left(m+\frac{\phi}{2\pi}\right)L-\frac{w}{2} \le & z \le \left(m+\frac{\phi}{2\pi}\right)L+\frac{w}{2}. \end{aligned}$$

- Region II, the interaction region

$$r_b \le r \le r_c.$$

- Region III, the outer groove space

$$\begin{aligned} r_c \le & r \le r_d, \\ \left(m+\frac{\phi}{2\pi}\right)L+S-\frac{W}{2} \le & z \le \left(m+\frac{\phi}{2\pi}\right)L+S+\frac{W}{2} \end{aligned}$$

where m is the order of the groove.

For the convenience of expressing the fields, in Region II, the cylindrical coordinates r, ϕ, and z are used, in Regions I and III, the helical coordinates r, θ, and ξ are employed. θ is along the helical direction. The direction of ξ is perpendicular to the directions of r and θ. The relationship between the two coordinate systems on the surface $r = r_b$ is shown in Fig. 2. It will be discussed in detail in Section II-C. The relationship on $r = r_c$ is similar.

A. Fields in the Interaction Region

Both the slow and fast waves may propagate in the interaction region due to the metal envelope of the structure. Expressed in TE and TM modes, the fields in the interaction region can be written as (1), shown at the bottom of this page, where γ_n and β_n are the radial and axial propagation constants of the nth space harmonic, respectively. n, ω, and μ_0 are the order of the space harmonics, angular frequency, and permeability of free space, respectively. k is the wavenumber in free space. If $\gamma_n^2 = k^2 - \beta_n^2 < 0$, the nth space harmonic represents the slow-wave mode, then $F_n(\gamma_n r) = I_n(\gamma_n r)$, $G_n(\gamma_n r) = K_n(\gamma_n r)$, and the upper sign of "$\pm$" or "$\mp$" in front of some expressions should be used. If $\gamma_n^2 = k^2 - \beta_n^2 > 0$, the nth space harmonic is the fast-wave mode, and then $F_n(\gamma_n r) = J_n(\gamma_n r)$, $G_n(\gamma_n r) = Y_n(\gamma_n r)$, and the lower sign of "$\pm$" or "$\mp$" is used. I_n and K_n represent the first and second types of modified Bessel functions of order n, respectively. J_n and Y_n are the first and second types of ordinary Bessel functions, respectively.

It should be noted that the axial and angular harmonic numbers in (1) are the same. This is because helical groove structures have periodicity in both axial and helical directions. With respect to the axial translation by a distance $z' < L$, the angular translation would be $(z'/L)2\pi$. Making use of this condition and Floquet theorem, it can be shown that the axial and angular harmonic numbers in (1) should be the same.

B. Fields in Regions I and III

In the grooves, the modes with higher orders are evanescent ones. Only the modes with a homogeneous electric field across the breadth of the grooves need to be taken into account [12]. We assuming waves in the grooves propagate along the helical direction. The longitudinal propagation constants for the modes with a homogeneous electric field across the breadth of the grooves are zeros, therefore, $\gamma_0 = k$. Waves in grooves are fast waves. Fields in regions I and III can be written as

$$\begin{cases} E_\xi^{I,III} = \left[A_\nu^{I,III}J_\nu(kr) + B_\nu^{I,III}J_{-\nu}(kr)\right]e^{-j\nu\theta} \\ H_r^{I,III} = \dfrac{\nu}{\omega\mu_0 r}\left[A_\nu^{I,III}J_\nu(kr) + B_\nu^{I,III}J_{-\nu}(kr)\right]e^{-j\nu\theta} \\ H_\theta^{I,III} = -j\dfrac{k}{\omega\mu_0}\left[A_\nu^{I,III}J'_\nu(kr) + B_\nu^{I,III}J'_{-\nu}(kr)\right]e^{-j\nu\theta} \\ E_r^{I,III} = E_\theta^{I,III} = H_\xi^{I,III} = 0 \end{cases} \tag{2}$$

where ν is the azimuthal propagation coefficient referring to the wavenumber in one revolution. When ν is an integer N, $J_{-\nu}(kr)$ in (2) should be replaced by $Y_N(kr)$. It is clear that

$$\beta_0 L = 2\pi\nu$$

$$\begin{cases} E_r^{II} = j\sum_{n=-\infty}^{\infty} \pm\left\{\gamma_n\beta_n\left[A_n^{II}F'_n(\gamma_n r) + B_n^{II}G'_n(\gamma_n r)\right] - \dfrac{n\omega\mu_0}{r}\left[C_n^{II}F_n(\gamma_n r) + D_n^{II}G_n(\gamma_n r)\right]\right\}e^{-j(\beta_n z - n\phi)} \\ E_\phi^{II} = \sum_{n=-\infty}^{\infty} \mp\left\{\dfrac{n\beta_n}{r}\left[A_n^{II}F_n(\gamma_n r) + B_n^{II}G_n(\gamma_n r)\right] - \omega\mu_0\gamma_n\left[C_n^{II}F'_n(\gamma_n r) + D_n^{II}G'_n(\gamma_n r)\right]\right\}e^{-j(\beta_n z - n\phi)} \\ E_z^{II} = \sum_{n=-\infty}^{\infty} \gamma_n^2\left[A_n^{II}F_n(\gamma_n r) + B_n^{II}G_n(\gamma_n r)\right]e^{-j(\beta_n z - n\phi)} \\ H_r^{II} = \sum_{n=-\infty}^{\infty} \pm\left\{\dfrac{nk^2}{\omega\mu_0 r}\left[A_n^{II}F_n(\gamma_n r) + B_n^{II}G_n(\gamma_n r)\right] - \gamma_n\beta_n\left[C_n^{II}F'_n(\gamma_n r) + D_n^{II}G'_n(\gamma_n r)\right]\right\}e^{-j(\beta_n z - n\phi)} \\ H_\phi^{II} = j\sum_{n=-\infty}^{\infty} \pm\left\{\dfrac{k^2\gamma_n}{\omega\mu_0}\left[A_n^{II}F'_n(\gamma_n r) + B_n^{II}G'_n(\gamma_n r)\right] - \dfrac{n\beta_n}{r}\left[C_n^{II}F_n(\gamma_n r) + D_n^{II}G_n(\gamma_n r)\right]\right\}e^{-j(\beta_n z - n\phi)} \\ H_z^{II} = j\sum_{n=-\infty}^{\infty} \gamma_n^2\left[C_n^{II}F_n(\gamma_n r) + D_n^{II}G_n(\gamma_n r)\right]e^{-j(\beta_n z - n\phi)} \end{cases} \tag{1}$$

and

$$\beta_n = \frac{2\pi(n+\nu)}{L}. \tag{3}$$

C. Conversion Between Cylindrical and Helical Coordinate Systems

Suppose φ_a, φ_b, φ_c, and φ_d are pitch angles on surfaces $r = r_a$, $r = r_b$, $r = r_c$, and $r = r_d$, respectively. If all the pitch angles are small enough, i.e., $\tan\varphi_a = L/(2\pi r_a) \ll 1$, $\tan\varphi_b = L/(2\pi r_b) \ll 1$, $\tan\varphi_c = L/(2\pi r_c) \ll 1$, $\tan\varphi_d = L/(2\pi r_d) \ll 1$, then θ can be measured by its projection on the plane perpendicular to the axis. In practice, period L is small compared with radii, thus, it is reasonable to measure θ by its projection.

It can be seen in (2) that electric fields in Regions I and III are independent of ξ, but they are related to θ and, therefore, to z. When matching conditions of the fields at boundaries are used, the relations between cylindrical and helical coordinates need to be known. As shown in Fig. 2, suppose coordinates θ and z at point P on the central line of the groove are $\theta_p = 2m\pi + \phi$ and $z_p = [m + \phi/(2\pi)]L$, respectively. Q is an arbitrary point at the axis on surface $r = r_b$. R is the projection of Q to the helical direction. Suppose the change of z from point P to point Q is z', then the variation for θ is

$$\Delta\theta = \frac{\overline{PR}\cos\varphi_b}{r_b} = \frac{z'\sin\varphi_b\cos\varphi_b}{r_b}$$

thus,

$$\theta = \theta_p + \Delta\theta = (2m\pi + \phi) + \frac{z'\sin\varphi_b\cos\varphi_b}{r_b}. \tag{4}$$

Expression (4) indicates the relation between cylindrical and helical coordinate systems on surface $r = r_b$. Their relation on surface $r = r_c$ is similar.

III. Dispersion Equation

To obtain the dispersion equation, the following boundary and matching conditions of fields are needed.

- Boundary condition on surface $r = r_a$

$$E_\xi^I \cos\varphi_a = 0. \tag{5}$$

- Boundary condition on surface $r = r_d$

$$E_\xi^{III} \cos\varphi_d = 0. \tag{6}$$

- Matching conditions of electric fields on surface $r = r_b$ are shown in (7) and (8) at the bottom of this page.
- Matching conditions of electric fields on surface $r = r_c$ are shown in (9) and (10) at the bottom of this page.
- Matching condition of magnetic fields on surface $r = r_b$

$$H_\phi^{II}\cos\varphi_b + H_z^{II}\sin\varphi_b = H_\theta^I. \tag{11}$$

- Matching condition of magnetic fields on surface $r = r_c$

$$H_\phi^{II}\cos\varphi_c + H_z^{II}\sin\varphi_c = H_\theta^{III}. \tag{12}$$

According to field expressions (2) and boundary conditions (5) and (6), field coefficients in regions I and III can be written as

$$\begin{aligned} A_v^I &= -E_0^I J_{-v}(kr_a) \\ B_v^I &= E_0^I J_v(kr_a) \\ A_\nu^{III} &= E_0^{III} J_{-\nu}(kr_d) \\ B_\nu^{III} &= -E_0^{III} J_\nu(kr_d) \end{aligned}$$

where E_0^I and E_0^{III} are ratio coefficients in regions I and III, respectively.

$$E_z^{II} = \begin{cases} E_\xi^I \cos\varphi_b & \left(m+\dfrac{\phi}{2\pi}\right)L - \dfrac{w}{2} \le z \le \left(m+\dfrac{\phi}{2}\right)L + \dfrac{w}{2} \\ 0 & \left(m+\dfrac{\phi}{2\pi}\right)L + \dfrac{w}{2} \le z \le \left(m+\dfrac{\phi}{2\pi}\right)L - \dfrac{w}{2} + L \end{cases} \tag{7}$$

$$E_\phi^{II} = \begin{cases} -E_\xi^I \sin\varphi_b & \left(m+\dfrac{\phi}{2\pi}\right)L - \dfrac{w}{2} \le z \le \left(m+\dfrac{\phi}{2}\right)L + \dfrac{w}{2} \\ 0 & \left(m+\dfrac{\phi}{2\pi}\right)L + \dfrac{w}{2} \le z \le \left(m+\dfrac{\phi}{2\pi}\right)L - \dfrac{w}{2} + L \end{cases} \tag{8}$$

$$E_z^{II} = \begin{cases} E_\xi^{III} \cos\varphi_c & \left(m+\dfrac{\phi}{2\pi}\right)L + S - \dfrac{W}{L} \le z \le \left(m+\dfrac{\phi}{2\pi}\right)L + S + \dfrac{W}{2} \\ 0 & \left(m+\dfrac{\phi}{2\pi}\right)L + S + \dfrac{W}{2} \le z \le \left(m+\dfrac{\phi}{2\pi}\right)L + S - \dfrac{W}{2} + L \end{cases} \tag{9}$$

$$E_\phi^{II} = \begin{cases} -E_\xi^{III} \sin\varphi_c & \left(m+\dfrac{\phi}{2\pi}\right)L + S - \dfrac{W}{L} \le z \le \left(m+\dfrac{\phi}{2\pi}\right)L + S + \dfrac{W}{2} \\ 0 & \left(m+\dfrac{\phi}{2\pi}\right)L + S + \dfrac{W}{2} \le z \le \left(m+\dfrac{\phi}{2\pi}\right)L + S - \dfrac{W}{2} + L \end{cases} \tag{10}$$

By making use of the above coefficients and (7)–(10), we can obtain the coefficients of fields in region II, as shown in (13)–(16) at the bottom of this page, where

$$M(x,y) = \frac{\sin\left[\frac{(n+\nu\cos^2 x)\pi y}{L}\right]}{\frac{(n+\nu\cos^2 x)\pi y}{L}}$$
$$P_v(x,y) = J_\nu(kx)J_{-v}(ky) - J_{-v}(kx)J_v(ky)$$
$$P_n(x,y) = F_n(\gamma_n x)G_n(\gamma_n y) - G_n(\gamma_n x)F_n(\gamma_n y)$$
$$\eta_n = e^{j2\pi nS/L}$$
$$T(x,y) = \frac{1}{\gamma_n k}\left(\pm\frac{n\beta_n}{x} - \gamma_n^2\tan y\right)$$
$$S_n(x,y) = F_n'(\gamma_n x)G_n'(\gamma_n y) - G_n'(\gamma_n x)F_n'(\gamma_n y).$$

Substituting (13)–(16) into (11), we can get the relation between E_0^I and E_0^{III}. Substituting (13)–(16) into (12) and using the relation between E_0^I and E_0^{III}, the dispersion equation is then finally derived as shown in (17) at the bottom of this page, where

$$U_w = \frac{wM(\varphi_b,w)P_v(r_a,r_b)\cos\varphi_b}{\gamma_n L}$$
$$U_W = \frac{WM(\varphi_c,W)P_v(r_c,r_d)\cos\varphi_c}{\gamma_n L}$$
$$R_n(x,y) = F_n'(\gamma_n x)G_n(\gamma_n y) - G_n'(\gamma_n x)F_n(\gamma_n y)$$
$$Q_n(x,y) = F_n(\gamma_n x)G_n'(\gamma_n y) - G_n(\gamma_n x)F_n'(\gamma_n y)$$
$$R_v(x,y) = J_{-v}(ky)J_\nu'(kx) - J_v(ky)J_{-v}'(kx)$$
$$Q_v(x,y) = J_\nu(kx)J_{-v}'(ky) - J_{-v}(kx)J_v'(ky)$$
$$S_w = \frac{\sin\left(\frac{\beta_n w}{2}\right)}{\frac{\beta_n w}{2}}$$
$$S_W = \frac{\sin\left(\frac{\beta_n W}{2}\right)}{\frac{\eta_n\beta_n W}{2}}.$$

The obtained dispersion equation [i.e., (17)] is a general form for helical-groove type circuits. It can be easily changed into the dispersion equations of the following three special cases:

1) helical-groove structure without an inner groove;
2) helical-groove structure with a coaxial inner conductor;
3) inner helical-groove structure with an outer cylinder (see Appendix).

IV. Coupling Impedance

In a TWT, coupling impedance, which is a measure of the coupling between the electric field and one electron beam in the interaction region for a given electromagnetic power, determines the coupling between the wave and beam. It is an important parameter for the gain and efficiency of a tube. From

$$A_n^{II} = \frac{1}{L\gamma_n^2}\left[\frac{wE_0^I M(\varphi_b,w)P_v(r_a,r_b)\cos\varphi_b G_n(\gamma_n r_c)}{P_n(r_b,r_c)} - \frac{WE_o^{III}\eta_n M(\varphi_c,W)P_v(r_c,r_d)\cos\varphi_c G_n(\gamma_n r_b)}{P_n(r_b,r_c)}\right] \quad (13)$$

$$B_n^{II} = \frac{1}{L\gamma_n^2}\left[\frac{WE_0^{III}\eta_n M(\varphi_c,W)P_v(r_c,r_d)\cos\varphi_c F_n(\gamma_n r_b)}{P_n(r_b,r_c)} - \frac{wE_o^I M(\varphi_b,w)P_v(r_a,r_b)\cos\varphi_b F_n(\gamma_n r_c)}{P_n(r_b,r_c)}\right] \quad (14)$$

$$C_n^{II} = \pm\frac{k}{\omega\mu_0\gamma_n^2}\left\{\frac{w}{L}E_0^I M(\varphi_b,w)P_v(r_a,r_b)G_n'(\gamma_n r_c)T(r_b,\varphi_b)\cos\varphi_b - \frac{W}{L}E_0^{III}\eta_n M(\varphi_c,W)P_v(r_c,r_d)G_n'(\gamma_n r_b)T(r_c,\varphi_c)\cos\varphi_c\right\}\frac{1}{S_n(r_b,r_c)} \quad (15)$$

$$D_n^{II} = \mp\frac{k}{\omega\mu_0\gamma_n^2}\left\{\frac{w}{L}E_0^I M(\varphi_b,w)P_v(r_a,r_b)F_n'(\gamma_n r_c)T(r_b,\varphi_b)\cos\varphi_b - \frac{W}{L}E_0^{III}\eta_n M(\varphi_c,W)P_v(r_c,r_d)F_n'(\gamma_n r_b)T(r_c,\varphi_c)\cos\varphi_c\right\}\frac{1}{S_n(r_b,r_c)} \quad (16)$$

$$\frac{\sum_{n=-\infty}^{\infty}\pm U_w\left[\frac{R_n(r_c,r_c)}{P_n(r_b,r_c)} - T(r_c,\varphi_c)T(r_b,\varphi_b)\frac{Q_n(r_c,r_c)}{S_n(r_b,r_c)}\right]\cos\varphi_c\frac{S_W}{\eta_n}}{\frac{Q_v(r_a,r_b)}{k} + \sum_{n=-\infty}^{\infty}\pm U_w\left[\frac{R_n(r_b,r_c)}{P_n(r_b,r_c)} - T^2(r_b,\varphi_b)\frac{Q_n(r_b,r_c)}{S_n(r_b,r_c)}\right]\cos\varphi_b Sw} = \frac{\frac{R_v(r_c,r_d)}{k} + \sum_{n=-\infty}^{\infty}\pm U_W\left[\frac{Q_n(r_b,r_c)}{P_n(r_b,r_c)} - T^2(r_c,\varphi_c)\frac{R_n(r_b,r_c)}{S_n(r_b,r_c)}\right]\cos\varphi_c S_W}{\sum_{n=-\infty}^{\infty}\pm U_W\eta_n\left[\frac{Q_n(r_b,r_b)}{P_n(r_b,r_c)} - T(r_c,\varphi_c)T(r_b,\varphi_b)\frac{R_n(r_b,r_b)}{S_n(r_b,r_c)}\right]\cos\varphi_b Sw} \quad (17)$$

Pierce's theory [13], the coupling impedance of the nth space harmonic is defined as

$$K_{cn} = \frac{E_{zn}E_{zn}^*}{2\beta_n^2 P} \tag{18}$$

where E_{zn} is the longitudinal component of the nth space harmonic at the position of the electron beam, and E_{zn}^* is its conjugate. P is the total power flow through the whole circuit

$$P = P^I + P^{III} + \sum_n P_n^{II}$$

where P^I and P^{III} are the power flows in regions I and III, respectively. P_n^{II} is the power flow of the nth space harmonic in region II.

According to (1), we have

$$E_{zn}^{II}\left(E_{zn}^{II}\right)^* = \gamma_n^4\left[A_n^{II}F_n(\gamma_n r) + B_n^{II}G_n(\gamma_n r)\right]^2. \tag{19}$$

Using the obtained expressions for the field coefficients, the power flow in each region can be written as follows:

$$\begin{aligned}
P^I =& \frac{1}{2}w\int_{r_a}^{r_b} E_\xi^I\left(H_r^I\right)^* dr \\
=& \frac{w}{4\omega\mu_0}\left(E_0^I\right)^2 \\
&\cdot\Bigg\{P_\nu^2(r_a,r_b) - kr_b\Big[J_{-\nu}(kr_a)J_{\nu+1}(kr_b) \\
&\qquad + J_\nu(kr_a)J_{-(\nu+1)}(kr_b)\Big] \\
&\cdot\frac{\partial}{\partial\nu}P_\nu(r_a,r_b) + kr_bP_\nu(r_a,r_b) \\
&\cdot\frac{\partial}{\partial\nu}\Big[J_{-\nu}(kr_a)J_{\nu+1}(kr_b) + J_\nu(kr_a)J_{-(\nu+1)}(kr_b)\Big]\Bigg\}
\end{aligned} \tag{20}$$

$$\begin{aligned}
P_n^{II} =& \frac{1}{2}2\pi\int_{r_b}^{r_c}\left[E_{rn}^{II}\left(H_{\phi n}^{II}\right)^* - E_{\phi n}^{II}\left(H_{rn}^{II}\right)^*\right]rdr \\
=& \frac{k^2\beta_n}{4\omega\mu_0}\pi(\gamma_n r)^2 \\
&\cdot\Big[\left(A_n^{II}F_{n-1} \mp B_n^{II}G_{n-1}\right)^2 + \left(A_n^{II}F_{n+1} \mp B_n^{II}G_{n+1}\right)^2 \\
&\quad - \left(A_n^{II}F_n + B_n^{II}G_n\right)\left(A_n^{II}F_{n-2} + A_n^{II}F_{n+2}\right. \\
&\qquad \left. + B_n^{II}G_{n-2} + B_n^{II}G_{n+2}\right)\Big]\Big|_{r_b}^{r_c} \\
&+ \frac{1}{4}\omega\mu_0\pi\beta_n(\gamma_n r)^2\Big[\left(C_n^{II}F_{n-1} \mp D_n^{II}G_{n-1}\right)^2 \\
&\qquad + \left(C_n^{II}F_{n+1} \mp D_n^{II}G_{n+1}\right)^2 \\
&\qquad - \left(C_n^{II}F_n + D_n^{II}G_n\right) \\
&\qquad \cdot\left(C_n^{II}F_{n-2} + C_n^{II}F_{n+2}\right. \\
&\qquad \left. + D_n^{II}G_{n-2} + D_n^{II}G_{n+2}\right)\Big]\Big|_{r_b}^{r_c} \\
&- n\pi(k^2+\beta_n^2)\Big[A_n^{II}C_n^{II}F_n^2 + B_n^{II}D_n^{II}G_n^2 \\
&\qquad + \left(B_n^{II}C_n^{II} + A_n^{II}D_n^{II}\right)G_nF_n\Big]\Big|_{r_b}^{r_c}
\end{aligned} \tag{21}$$

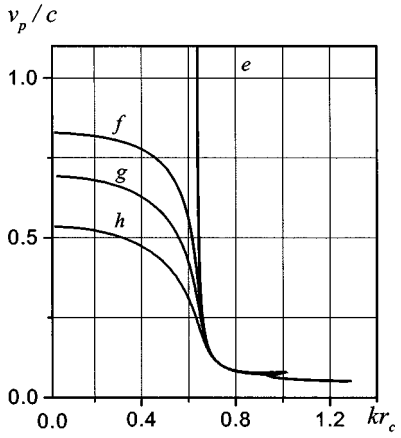

Fig. 3. Dispersion curves for a helical waveguide (for comparison with [10]) $r_d/r_c = 4.0$, $L/r_c = 0.5$, $w/L = W/L = 0.4$ e: $r_a/r_c = r_b/r_c = 0.0$; f: $r_a/r_c = r_b/r_c = 0.3$; g: $r_a/r_c = r_b/r_c = 0.6$; h: $r_a/r_c = r_b/r_c = 0.8$.

To shorten (21), $F_n(\gamma_n r)$, $G_n(\gamma_n r)$, etc., are written as F_n, G_n, etc.,

$$\begin{aligned}
P^{III} =& \frac{1}{2}W\int_{r_c}^{r_d} E_\xi^{III}\left(H_r^{III}\right)^* dr \\
=& -\frac{W}{4\omega\mu_0}\left(E_0^{III}\right)^2 \\
&\cdot\Big\{P_\nu^2(r_c,r_d) + kr_c\Big[J_{-\nu}(kr_d)J_{\nu+1}(kr_c) \\
&\qquad + J_\nu(kr_d)J_{-(\nu+1)}(kr_c)\Big] \\
&\cdot\frac{\partial}{\partial\nu}P_\nu(r_c,r_d) - kr_cP_\nu(r_c,r_d) \\
&\cdot\frac{\partial}{\partial\nu}\Big[J_{-\nu}(kr_d)J_{\nu+1}(kr_c) \\
&\qquad + J_\nu(kr_d)J_{-(\nu+1)}(kr_c)\Big]\Big\}
\end{aligned} \tag{22}$$

In the process of deriving P^I and P^{III}, some relevant integral formulas of Bessel functions are used. Substituting (19)–(22) into (18), the expression of the coupling impedance for a coaxial helical-groove circuit can be written out directly.

Similarly, the expressions of the coupling impedance for the three special cases can also be derived (see Appendix).

V. Results of Numerical Calculations

The dispersion relation, i.e., (17), is a very complex transcendental equation including the integrals of different types of Bessel functions and the summations of infinite series. Fortunately, the series converges rapidly as n increases. Considering only four terms, i.e., $n = -2, -1, 0$, and 1, we can get solution with a relative error of less than 10^{-6}. In the practical calculations, seven terms were taken into account. To verify our calculation, we compared our results with Foulds and Mansell's report [10] for a special case of the coaxial helical-groove structure, i.e., a helical-groove structure with a coaxial inner conductor. Fig. 3 shows our calculated curves. They are the same as [10, Fig. 25].

Using the data from the calculation of dispersion relation, we calculated coupling impedance according to (18). The coupling impedance is calculated by assuming that a thin electron beam

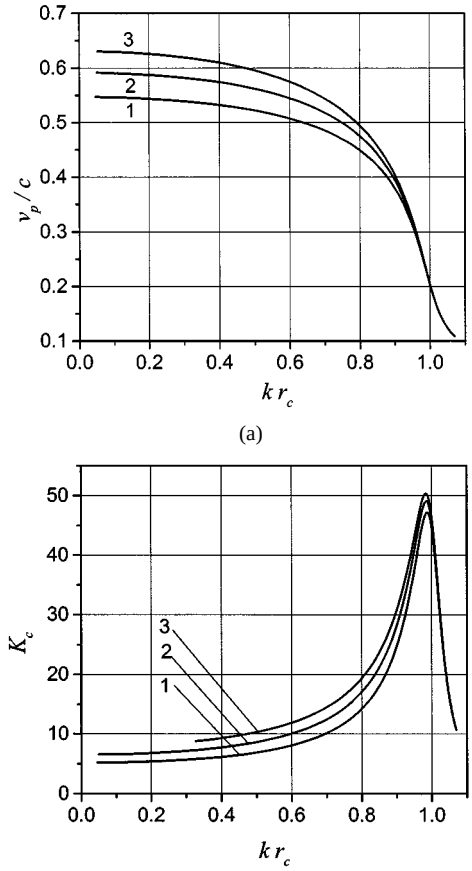

Fig. 4. Dispersion curve and coupling impedance change with parameter r_a (a) Dispersion curves. (b) Coupling impedance $r_b/r_c = 0.71$, $r_d/r_c = 2.86$, $L/r_c = 0.36$, $w = W = 0.14$, $S = 0.0$ 1: $r_a/r_c = 0.29$; 2: $r_a/r_c = 0.43$; 3: $r_a/r_c = 0.57$.

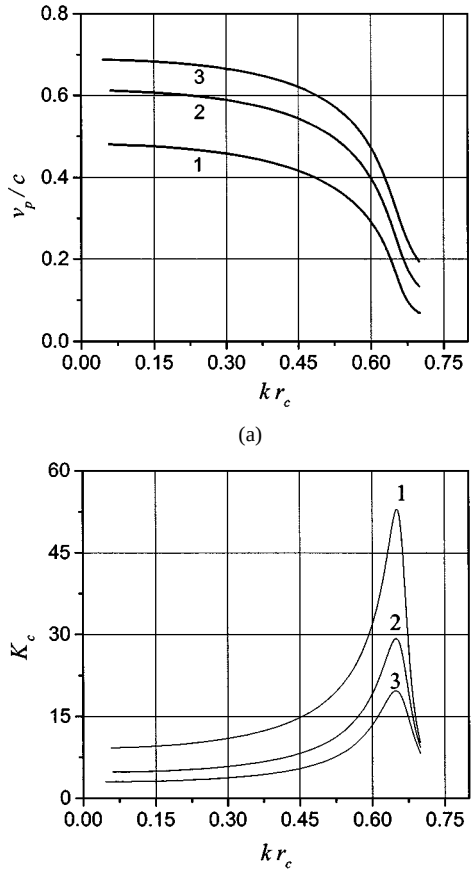

Fig. 5. Dispersion curve and coupling impedance change with parameter L (a) Dispersion curves. (b) Coupling impedance $r_a/r_c = 0.5$, $r_b/r_c = 0.8$, $r_d/r_c = 4.0$, $w = W = 0.1$, $S = 0.0$ 1: $L/r_c = 0.25$; 2: $L/r_c = 0.5$; 3: $L/r_c = 0.75$.

moves along the ports of the outer groove, i.e., the radius of the electron beam is equal to r_c, except in the case of the inner groove with an outer cylinder where the radius of the electron beam is supposed to be r_b. All the impedance curves refer to zeroth-order space harmonic.

The calculation results are described as follows. The normalized phase velocity and coupling impedance varying with radius r_a are given in Fig. 4(a) and (b), respectively. It is clear in Fig. 4(a) that phase velocity increases with r_a. This is easy to be understood. With the increase of r_a, the inner groove becomes shallower. If both the inner and outer grooves become shallower and shallower, the structure approaching a coaxial line, and then the normalized phase velocity should approach one. Obviously, the shallower the grooves, the higher the phase velocity. It is consistent with our calculation. By the phase velocity changing with frequency (or wavenumber), the cold bandwidth of a structure can be estimated. Within the operation region, the more slowly the phase velocity changes with frequency, the wider the bandwidth. It is clear in Fig. 4(a) that with the increase of r_a, the bandwidth decrease. In Fig. 4(b), the increase of coupling impedance with r_a is also understandable because the fields are pushed into the interaction region by increasing r_a.

The influences of the structure period on the slow-wave characteristics are indicated in Fig. 5(a) and (b). As shown in Fig. 5(a), with the increase of period L, the phase velocity rises and the rate of phase velocity changing with frequency increase a little, therefore the bandwidth decrease a little. The coupling impedance drops with the increase of period, as shown in Fig. 5(b).

Fig. 6 is an optimum calculation result, i.e., the bandwidth is optimized while keeping the coupling impedance equal or larger than 16 Ω. It can be seen from Fig. 6(a) that for kr_c changing from 0.167 to 0.310, the phase velocity changes from 0.484 to 0.460; the variation compared with mean value, 0.472, is less than 5%. If calculated according to this variation, the cold bandwidth reaches 60% $(2*(0.310-0.167)/(0.310+0.167))$. Meanwhile, as shown in Fig. 6(b), the coupling impedance of the zeroth-order space harmonic is greater than 16 Ω. On the other hand, the coupling impedance of the -1 space harmonic is very small, and this behavior is very important for TWTs.

Fig. 7(a) and (b) is a comparison between a coaxial helical-groove structure and a noncoaxial one. Curve 1 is for the coaxial helical-groove circuit and curve 2 is for the noncoaxial circuit. It is obvious in Fig. 7(a) that the phase velocity of the coaxial helical-groove structure changes much more slowly than that of the noncoaxial helical-groove structure, therefore, the bandwidth of the coaxial helical-groove circuit is much broader. Numerical calculations also show that the two special coaxial structures, i.e., the: 1) helical-groove structure with a coaxial inner conductor and 2) inner helical-groove structure with an outer

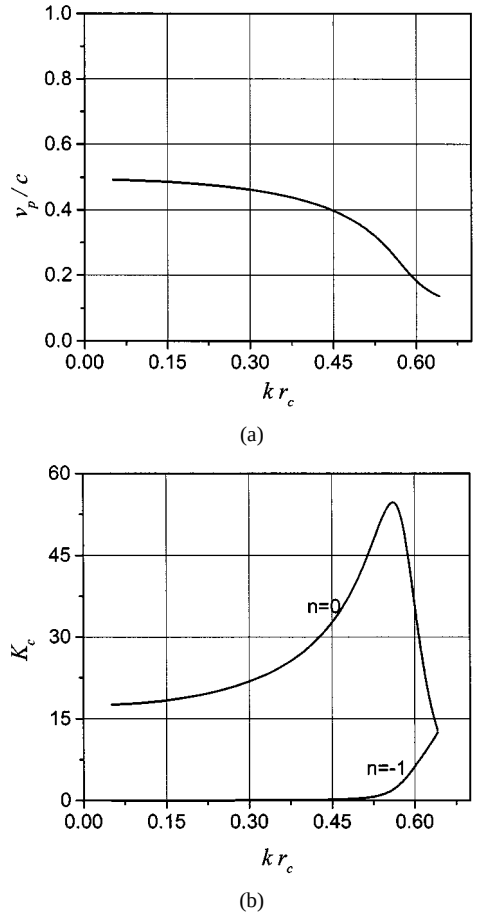

Fig. 6. Calculation of optimized bandwidth while keeping coupling impedance larger than 16 Ω (a) Dispersion curves. (b) Coupling impedance $r_a/r_c = 0.44, r_b/r_c = 0.67, r_d/r_c = 4.44, L/r_c = 0.67, w = W = 0.44, S = 0.0$.

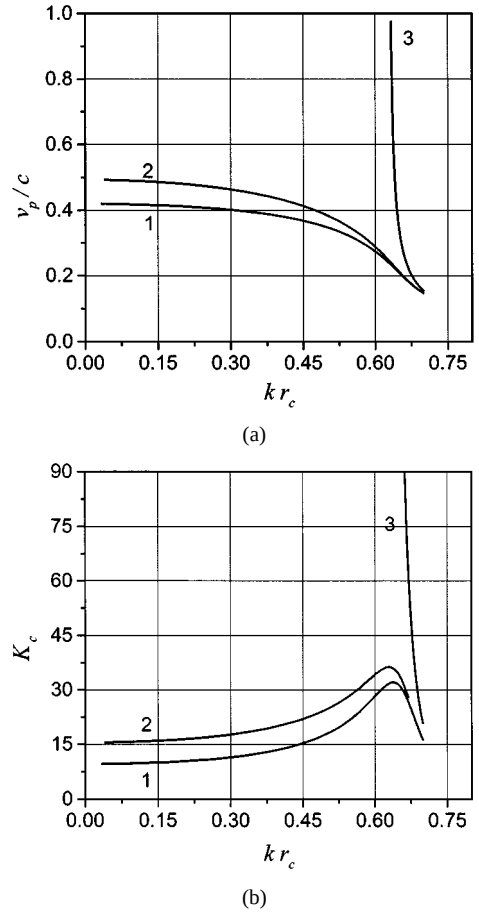

Fig. 7. Comparison between the coaxial helical-groove structure and its two special cases. (a) Dispersion curves. (b) Coupling impedance $r_c = 1.0, r_d = 4.0, L = 0.6, w = W = 0.3$ 1: $r_a = 0.4, r_b = 0.8$; 2: $r_a = r_b = 0.8$; 3: $r_a = r_b = 0.0$.

cylinder, can also reach broader bandwidth. The most distinguishing difference between the coaxial helical-groove structure and these two special cases are that the phase velocity of the coaxial helical-groove structure is lower and easier to adjust. The bandwidth of the coaxial helical-groove structure is a little broader. Fig. 7(b) shows that, at its narrow operation frequency range, the noncoaxial helical-groove structure has a higher coupling impedance.

From the above analysis, it can be seen that the coaxial helical-groove structure has a low dispersion, namely, it has a large potential application in broad-band TWTs. However, compared to a coupled-cavity structure [14], the value of the coupling impedance is relatively low, which would lead to a decrease in the gain and efficiency of the device. The coupling impedance of this type of structures can be increased to some extent by ridge loading at the inner groove mouth [15].

VI. Summary

The coaxial helical-groove structure has presented in this paper. Its dispersion characteristic and coupling impedance are analyzed by the field-matching method. The obtained expressions of the dispersion relation and coupling impedance are general forms, and they can be easily changed into those of the three special cases. The calculated results of normalized phase velocity and coupling impedance varying with some structural dimensions are given and analyzed. Calculation results show that the cold bandwidth of the coaxial helical-groove circuit can reach 60%; meanwhile, its coupling impedance is more than 16 Ω. As it is an all-metal structure, its power capacity should be high. Therefore, the coaxial helical-groove structure presented and analyzed in this paper is suitable for broad-band and high-power TWTs.

Appendix
Expressions of Dispersion Relations, Longitudinal Electrical Fields, and Power Flows for the Three Special Cases of a Coaxial Helical-Groove Structure

A. Helical-Groove Structure Without an Inner Helical Groove

Since there is not an inner helical groove, in this type of structure

$$\begin{aligned} r_a &= r_b = 0 \\ w &= S = 0 \\ A_\nu^I &= B_\nu^I = 0 \\ B_n^{II} &= D_n^{II} = 0 \\ A_n^{II} &= \frac{W}{L} E_0^{III} M(\varphi_c, W) P_\nu(r_c, r_d) \frac{\cos\varphi_c}{\gamma_n^2 F_n(\gamma_n r_c)} \end{aligned} \tag{A-1}$$

and

$$C_n^{II} = \pm\frac{\cos\varphi_c k}{\omega u_0 \gamma_n^2}\frac{W}{L}E_0^{III}M(\varphi_c, W)P_\nu(r_c, r_d)\frac{T(r_c,\varphi_c)}{F_n'(\gamma_n r_c)}. \tag{A-2}$$

The dispersion equation becomes

$$\frac{R_\nu(r_c,r_d)}{p_\nu(r_c,r_d)} + \frac{W}{L}\sum_{n=-\infty}^{\infty}\pm\frac{k}{\gamma_n}\left\{\frac{F_n'(\gamma_n r_c)}{F_n(\gamma_n r_c)} - T^2(r_c\gamma_c)\frac{F_n(\gamma_n r_c)}{F_n'(\gamma_n r_c)}\right\}(S_W)^2 = 0. \tag{A-3}$$

It is the same as that given by Foulds and Mansell in [10].

The expression for $E_{zn}E_{zn}^*$ can be written as

$$E_{zn}E_{zn}^* = \left[\frac{W}{L}M(\varphi_c,W)\cos\varphi_c P_\nu(r_c,r_d)\frac{F_n(\gamma_n r)}{F_n(\gamma_n r_c)}E_0^{III}\right]^2. \tag{A-4}$$

The power flows in the three regions are

$$P^I = 0 \tag{A-5}$$

$$\begin{aligned} P_n^{II} =& \left[\frac{k^2\beta_n}{4\omega\mu_0}\pi(\gamma_n r)^2\left(A_n^{II}\right)^2\right. \\ &\cdot\left(F_{n-1}^2 + F_{n+1}^2 - F_nF_{n-2} - F_nF_{n+2}\right) \\ &+\frac{\beta_n}{4}\omega\mu_0\pi(\gamma_n r)^2\left(C_n^{II}\right)^2 \\ &\cdot\left(F_{n-1}^2 + F_{n+1}^2 - F_nF_{n-2} - F_nF_{n+2}\right) \\ &\left.-n\left(k^2+\beta_n^2\right)\pi A_n^{II}C_n^{II}F_n^2\right]\Big|_0^{r_c} \end{aligned} \tag{A-6}$$

where A_n^{II} and C_n^{II} are given by (A-1) and (A-2), respectively. To shorten (A-6), $F_n(\gamma_n r)$, $F_{n-1}(\gamma_n r)$, etc. are written as F_n, F_{n-1}, etc.

P^{III} has the same form as (22) in Section III.

B. Helical-Groove Structure With a Coaxial Inner Conductor

In this type of structure, $w = S = 0$, $A_\nu^I = B_\nu^I = 0$, but $r_a = r_b \neq 0$. Thus, in the expressions of fields, there exist not only the first type of Bessel function, but also the second type. The coefficients of fields are simplified as

$$\begin{cases} A_n^{II} = A_0^{II}G_n(\gamma_n r_b) \\ B_n^{II} = -A_0^{II}F_n(\gamma_n r_b) \\ C_n^{II} = C_0^{II}G_n'(\gamma_n r_b) \\ D_n^{II} = -C_0^{II}F_n'(\gamma_n r_b) \end{cases} \tag{A-7}$$

where

$$A_0^{II} = -\frac{W}{L}E_0^{III}M(\varphi_c,W)\frac{P_\nu(r_c,r_d)\cos\varphi_c}{P_n(r_b,r_c)\gamma_n^2} \tag{A-8}$$

$$C_0^{II} = \mp\frac{W}{L}E_0^{III}M(\varphi_c,W)\frac{P_\nu(r_c,r_d)}{S_n(r_b,r_c)}\frac{k\cos\varphi_c}{\gamma_n^2\omega\mu_0}T(r_c,\varphi_c). \tag{A-9}$$

The dispersion equation can be written as

$$\frac{R_\nu(r_c,r_d)}{p_\nu(r_c,r_d)} + \frac{W}{L}\sum_{n=-\infty}^{\infty}\pm\frac{k}{\gamma_n}\left\{\frac{Q_n(r_b,r_c)}{P_n(r_b,r_c)} - T(r_c,\varphi_c)^2\frac{R_n(r_b,r_c)}{S_n(r_b,r_c)}\right\}\cos^2\varphi_c S_W^2 = 0. \tag{A-10}$$

It is identical with the result obtained by Henoch in [12].

The expression for $E_{zn}E_{zn}^*$ is

$$E_{zn}E_{zn}^* = \left[\frac{W}{L}M(\varphi_c,W)\cos\varphi_c P_\nu(r_c,r_d)E_0^{III}\right]^2 \cdot\frac{P_n^2(r_b,r)}{P_n^2(r_b,r_c)}. \tag{A-11}$$

The power flows in the three regions are

$$P^I = 0 \tag{A-12}$$

$$\begin{aligned} P_n^{II} =& \frac{k^2|\hat{A}_n}{4\omega\mu_0}\pi(\gamma_n r)^2\left(A_0^{II}\right)^2 \\ &\cdot\left\{\left[G_n(\gamma_n r_b)F_{n-1} \pm F_n(\gamma_n r_b)G_{n-1}\right]^2\right. \\ &\quad+\left[G_n(\gamma_n r_b)F_{n+1} \pm F_n(\gamma_n r_b)G_{n+1}\right]^2 - P_n(r_b,r) \\ &\quad\cdot\left[G_n(\gamma_n r_b)F_{n-2} - F_n(\gamma_n r_b)G_{n-2}\right. \\ &\quad\left.\left.+G_n(\gamma_n r_b)F_{n+2} - F_n(\gamma_n r_b)G_{n+2}\right]\right\}\Big|_{r_b}^{r_c} \\ &+\frac{1}{4}\omega\mu_0\beta_n\pi(\gamma_n r)^2\left(C_0^{II}\right)^2 \\ &\cdot\left\{\left[G_n'(\gamma_n r_b)F_{n-1} \pm F_n'(\gamma_n r_b)G_{n-1}\right]^2\right. \\ &\quad+\left[G_n'(\gamma_n r_b)F_{n+1} \pm F_n'(\gamma_n r_b)G_{n+1}\right]^2 + R_n(r_b,r) \\ &\quad\cdot\left[G_n'(\gamma_n r_b)F_{n-2} - F_n'(\gamma_n r_b)G_{n-2}\right. \\ &\quad\left.\left.+G_n'(\gamma_n r_b)F_{n+2} - F_n'(\gamma_n r_b)G_{n+2}\right]\right\}\Big|_{r_b}^{r_c} \\ &-n(k^2+\beta_n^2)\pi A_0^{II}C_0^{II} \\ &\cdot\left\{\left[G_n(\gamma_n r_b)G_n'(\gamma_n r_b)F_n^2 + F_n(\gamma_n r_b)F_n'(\gamma_n r_b)G_n^2\right]\right. \\ &\quad-\left[G_n(\gamma_n r_b)F_n'(\gamma_n r_b)\right. \\ &\quad\left.\left.+F_n(\gamma_n r_b)G_n'(\gamma_n r_b)\right]F_nG_n\right\}\Big|_{r_b}^{r_c} \end{aligned} \tag{A-13}$$

where A_0^{II} and C_0^{II} are given by (A-8) and (A-9). P^{III} has the same form as (22) in Section III.

C. Inner Helical-Groove Structure With an Outer Cylinder

In this case, $r_c = r_d$, $W = S = 0$, and $A_\nu^{III} = B_\nu^{III} = 0$. The boundary condition on surface $r = r_c$ is $E_z^{II} = E_\phi^{II} = 0$. Making use of this condition, we can get

$$\begin{cases} A_n^{II} = B_0^{II}G_n(\gamma_n r_c) \\ B_n^{II} = -B_0^{II}F_n(\gamma_n r_c) \\ C_n^{II} = D_0^{II}G_n'(\gamma_n r_c) \\ D_n^{II} = -D_0^{II}F_n'(\gamma_n r_c) \end{cases} \tag{A-14}$$

where

$$B_0^{II} = \frac{w}{L}\frac{1}{\gamma_n^2}E_0^I M(\varphi_b, w)\cos\varphi_b \frac{P_\nu(r_a, r_b)}{P_n(r_b, r_c)} \tag{A-15}$$

$$D_0^{II} = \pm\frac{w}{L}E_0^I M'(\varphi_b, w)\frac{k\cos\varphi_b}{\gamma_n^2\omega\mu_0}T(r_b, \varphi_b)\frac{P_\nu(r_a, r_b)}{S_n(r_b, r_c)}. \tag{A-16}$$

The dispersion equation now becomes

$$\frac{Q_\nu(r_a, r_b)}{p_\nu(r_a, r_b)} + \frac{w}{L}\sum_{n=-\infty}^{\infty}\pm\frac{k}{\gamma_n}\left\{\frac{R_n(r_b, r_c)}{P_n(r_b, r_c)} - T^2(r_b, \varphi_b)\frac{Q_n(r_b, r_c)}{S_n(r_b, r_c)}\right\} \cdot\cos^2\varphi_b S_w^2 = 0. \tag{A-17}$$

We have not seen a report about this type of structure.

The expression for $E_{zn}E_{zn}^*$ is

$$E_{zn}E_{zn}^* = \left[\frac{w}{L}M(\varphi_b, w)\cos\varphi_b P_\nu(r_a, r_b)E_0^I\right]^2\frac{P_n^2(r, r_c)}{P_n^2(r_b, r_c)}. \tag{A-18}$$

The power flows in the three regions are as follows. P^I has the same form as (20) in Section III as follows:

$$\begin{aligned}
P_n^{II} =& \frac{k^2\beta_n}{4\omega\mu_0}\pi(\gamma_n r)^2\left(B_0^{II}\right)^2 \\
&\cdot\Big\{\left[G_n(\gamma_n r_d)F_{n-1} \pm F_n(\gamma_n r_d)G_{n-1}\right]^2 \\
&\quad + \left[G_n(\gamma_n r_d)F_{n+1} \pm F_n(\gamma_n r_d)G_{n+1}\right]^2 - P_n(r, r_d) \\
&\quad \cdot\left[G_n(\gamma_n r_d)F_{n-2} - F_n(\gamma_n r_d)G_{n-2}\right. \\
&\qquad \left.+G_n(\gamma_n r_d)F_{n+2} - F_n(\gamma_n r_d)G_{n+2}\right]\Big\}\Big|_{r_b}^{r_c} \\
&+ \frac{1}{4}\omega\mu_0\beta_n\pi(\gamma_n r)^2\left(D_0^{II}\right)^2 \\
&\cdot\Big\{\left[G_n'(\gamma_n r_d)F_{n-1} \pm F_n'(\gamma_n r_d)G_{n-1}\right]^2 \\
&\quad + \left[G_n'(\gamma_n r_d)F_{n+1} \pm F_n'(\gamma_n r_d)G_{n+1}\right]^2 - Q_n(r, r_d) \\
&\quad \cdot\Big[G_n'(\gamma_n r_d)F_{n-2} - F_n'(\gamma_n r_d)G_{n-2} \\
&\qquad + G_n'(\gamma_n r_d)F_{n+2} - F_n'(\gamma_n r_d)G_{n+2}\Big]\Big\}\Big|_{r_b}^{r_c} \\
&- n\left(k^2 + \beta_n^2\right)\pi B_0^{II}D_0^{II} \\
&\cdot\Big\{\Big[G_n(\gamma_n r_d)G_n'(\gamma_n r_d)F_n^2 + F_n(\gamma_n r_d)F_n'(\gamma_n r_d)G_n^2\Big] \\
&\quad - \Big[G_n(\gamma_n r_d)F_n'(\gamma_n r_d) \\
&\qquad + F_n(\gamma_n r_d)G_n'(\gamma_n r_d)\Big]F_n G_n\Big\}\Big|_{r_b}^{r_c}
\end{aligned} \tag{A-19}$$

$$P^{III} = 0. \tag{A-20}$$

Substituting the power flows and longitudinal field components into (18) in Section IV, the coupling impedance for each special case can be obtained directly.

REFERENCES

[1] W. X. Wang, G. F. Yu, and Y. Y. Wei, "Study of the ridge-loaded helical-groove slow-wave structure," *IEEE Trans. Microwave Theory Tech.*, vol. 45, pp. 1689–1695, Oct. 1997.

[2] M. Takahashi, T. Yamaguchi, H. Hashimoto, T. Konishi, and H. Sato, "Non-brazed helix TWT attained 3 kW output at C-band and 600 W at Ku-band," in *Int. Electron Devices Meeting*, 1986, pp. 167–170.

[3] J. C. Kuntzmann and P. Nugues, "High power, high efficiency wideband TWT's," in *Int. Electron Devices Meeting*, 1986, pp. 171–173.

[4] P. K. Jain and B. N. Basu, "The inhomogeneous loading effects of a practical dielectric supports for the helical slow-wave structure of a TWT," *IEEE Trans. Electron Devices*, vol. ED-36, pp. 2643–2638, Dec. 1987.

[5] L. Kumar, R. S. Raju, S. N. Joshi, and B. N. Basu, "Modeling of a vane-loaded helical slow-wave structure for broad-band traveling-wave tubes," *IEEE Trans. Electron Devices*, vol. 36, pp. 1991–1999, Sept. 1989.

[6] D. Chernin, T. M. Antonsen, and B. Levush, "Exact treatment of dispersion and beam interaction impedance of a thin tape helix surrounded by a radially stratified dielectric," *IEEE Trans. Microwave Theory Tech.*, vol. 46, pp. 1472–1483, July 1999.

[7] B. G. James, "Coupled-cavity TWT design for future MM-wave system," *Microwave Syst. News Commun. Technol.*, pp. 105–106, Sept. 1986.

[8] L. M. Field, "Some slow-wave structure for TWT," *Proc. IRE*, vol. 37, pp. 34–40, Jan. 1949.

[9] M. A. Nwachuku, "The helical waveguide as a periodic structure for millimeter wave," Ph.D. dissertation, Dept. Elect. Eng., Univ. London, London, U.K., 1961.

[10] K. W. H. Foulds and J. R. Mansell, "Propagation of an electromagnetic wave through a helical waveguide," *Proc. Inst. Elect. Eng.*, vol. 111, pp. 1789–1798, Nov. 1964.

[11] G. G. Denisov, V. L. Bratman, A. D. R. Pheps, and S. V. Samsonov, "Gyro-TWT with a helical operating waveguide: New possibilities to enhance efficiency and frequency bandwidth," *IEEE Trans. Plasma Sci.*, vol. 26, pp. 508–518, June 1998.

[12] B. T. Henoch, "Investigations of the disk-loaded and helical waveguides," *J. Appl. Phys.*, vol. 18, no. 129, pp. 1–83, May 1958.

[13] J. R. Pierce, *Travelling Wave Tubes*. New York: Van Nostrand, 1950.

[14] J. F. Gittins, *Power Travelling Wave Tubes*. New York: American Elsevier, 1965.

[15] C. Liss, R. Harper, and M. P. Puri, "Helical waveguide millimeter wave TWT," in *Int. Electron Devices Meeting*, San Francisco, CA, Dec. 11–14, 1988, pp. 374–377.

Guofen Yu received the B.S. degree in applied physics from the National University of Defense Science and Technology, Changshu, China, in 1987, and the M.S. and Ph.D. degrees in physical electronics from the University of Electronics Science and Technology of China (UESTC), Chengdu, Sichuan, China, in 1990 and 1998, respectively.

Since 1990, she has been with the UESTC, where her research concerns microwave sources such as TWTs, gyrotrons, vircators, and high-power microwaves. From March 1999 to December 2000, she was a Post-Doctoral Associate in the Department of Electrical and Computer Engineering, Old Dominion University, Norfolk, VA, where she was involved with microwave effects on biological cells.

Wenxiang Wang was born in Jiansu Province, China, on July 24, 1940. He received the Engineering degree from the Chengdu Institute of Radio Engineering [now the University of Electronic Science and Technology of China (UESTC)], Chengdu, Sichuan, China, in 1963.

Since 1963, he has been with the Institute of High Energy Electronics, UESTC, where he is currently a Professor. From 1963 to 1978, he was engaged in the field of microwave electronic tubes including TWTs, continuous wave (CW) magnetrons, forward-wave amplifiers, etc. Since 1979, his research has concerned gyrotron high-power microwave tubes and techniques. From October 1986 to November 1988, he was a Visiting Scholar with the Plasma Research Laboratory, University of Maryland at College Park, where he investigated and designed a high-power mode-selective directional coupler for gyroklystron.

Prof. Wang is a committee member of the Chinese Vacuum Electronics Society and is a senior member of the Chinese Institute of Electronics.

Yanyu Wei was born in 1971. He received the B.S. degree in nuclear electronics and application of nuclear technology from the Mid-Southern Institute of Technology, Heng-yang, China, in 1993, and the M.Eng. and Ph.D. degrees in physical electronics from the University of Electronics Science and Technology of China (UESTC), Chengdu, Sichuan, China, in 1996 and 2000, respectively.

He is currently a Post-Doctoral Research Fellow at the Institute of High Energy Electronics, UESTC. His current research interests are mainly focused on nonlinear interaction of microwaves with plasma, novel high-power microwave amplifiers including helical groove TWTs, plasma-filled microwave sources, fast-wave microwave sources (particularly gyrotrons) in helical groove waveguide, and free electron lasers (FELs).

Shenggang Liu, photograph and biography not available at time of publication.